Jahn-Teller and Non-Jahn-Teller Systems Involving CuF64- Units: Role of the Internal Electric Field in Ba2ZnF6:Cu2+ and Other Insulating Systems

Aramburu, J. A.; Garcia-Fernandez, P.; García Lastra, Juan Maria; Moreno, M.

Published in:
Journal of Physical Chemistry C

Link to article, DOI:
10.1021/acs.jpcc.6b11999

Publication date:
2017

Document Version
Peer reviewed version

Jahn-Teller and Non-Jahn-Teller Systems Involving CuF_6^{4-} Units: Role of the Internal Electric Field in $Ba_2ZnF_6:Cu^{2+}$ and Other Insulating Systems

J.A. Aramburu*[1], P. García-Fernández[1], J. M. García-Lastra[2], and M. Moreno[1]

[1]*Departamento de Ciencias de la Tierra y Física de la Materia Condensada, Universidad de Cantabria, Avenida de los Castros s/n, 39005 Santander, Spain*

[2]*Center for Atomic-Scale Materials Design, Department of Physics, Technical University of Denmark, DK-2800 Kongens Lyngby, Denmark*

*(J.A.A.) E-mail: aramburj@unican.es

Abstract

The applicability of the Jahn-Teller (JT) framework to sixfold coordinated d^9 ions whose local symmetry is not strictly octahedral is explored by means of first principle calculations. Our results contradict much of the existing literature where these systems are analyzed within the quasi-JT regime which assumes the usual JT description with a small splitting between $b_{1g}(\sim x^2-y^2)$ and $a_{1g}(\sim 3z^2-r^2)$ orbitals and also the existence of three nearly equivalent distortions. To clarify this issue we investigate the equilibrium geometry (equatorial, R_{eq}, and axial, R_{ax}, Cu^{2+}-F^- distances) and optical transitions for CuF_6^{4-} units formed in Cu^{2+}-doped the tetragonal Ba_2ZnF_6 host lattice. While the experimental *d-d* transitions cannot be reproduced through the *isolated* CuF_6^{4-} unit at the equilibrium geometry, a reasonable agreement is reached adding in the calculation the internal electric field, $\mathbf{E}_R(\mathbf{r})$, created by the rest of lattice ions on the electrons confined in the complex. It is shown that this tetragonal field, $\mathbf{E}_R(\mathbf{r})$, already produces a gap $\Delta_0 \sim 0.35$ eV between $b_{1g}(\sim x^2-y^2)$ and $a_{1g}(\sim 3z^2-r^2)$ orbitals of $Ba_2ZnF_6:Cu^{2+}$ when $R_{ax} = R_{eq}$. Nevertheless, as this internal field leads to a Δ_0 value higher than typical JT barriers it drastically modifies the characteristic pattern of a JT effect. In particular, it prevents the existence of three equivalent distortions as confirmed by experimental EPR data. Furthermore, $\mathbf{E}_R(\mathbf{r})$ is shown to be the main physical reason behind an unusual compressed ground state with the hole in the $a_{1g}(\sim 3z^2-r^2)$ level while it is always placed in the $b_{1g}(\sim x^2-y^2)$ level for MX_6 complexes ($M = Cu^{2+}, Ag^{2+}, Ni^+$; $X = F^-, Cl^-$) in cubic lattices displaying a static JT effect. While the experimental results of CuF_6^{4-} in Ba_2ZnF_6 cannot be understood within the JT framework it is pointed out that a quasi-JT situation can however happen for a d^9 ion in a cubic lattice under a strain of $\sim 10^{-3}$ in agreement with experimental data. The present results stress the key role played by the internal electric fields for a quantitative understanding of compounds with transition metal cations. Moreover, they also demonstrate that in the interpretation of experimental data the use of a simple model should be avoided unless all its assumptions are well justified.

INTRODUCTION

In 1937 Jahn and Teller[1] explored the structural stability of molecules and solids showing that, when the electronic ground state is orbitally degenerate, the initial structure becomes unstable, with the only exception of linear molecules. To be more specific this idea just means that adiabatic minima displaying a lower symmetry than the initial one are, in general, found when orbital degeneracy comes out[2].

The Jahn-Teller (JT) effect has been widely invoked in the last fifty years for explaining the properties of systems involving d^9, d^7 and d^4 cations under octahedral coordination. Accordingly, experimental results on Cu^{2+} systems like superconducting copper oxides or copper oxyfluorides and on silver(II) fluorides have often been analyzed assuming the existence of a JT effect[3-11]. Nevertheless, this assumption implies that there exist a high symmetry reference conformation possessing an orbitally degenerate electronic state, but this crucial condition has not been proved in all cases[2, 12]. So, while it is fulfilled for the polaron in AgCl[13-15] and d^9 impurities in cubic lattices without any close defect[16-18], doubts have been raised analyzing the experimental and theoretical results for CuF_6^{4-} complexes in the *tetragonal* K_2ZnF_4 lattice[11, 19-22]. Indeed, the ground state in $K_2ZnF_4:Cu^{2+}$ is certainly unusual when compared to cubic fluoride[16, 23-27] or chloride lattices[28-33] doped with d^9 ions displaying a static JT effect. In the latter systems the hole is always in the $b_{1g}(\sim x^2-y^2)$ level while it surprisingly resides in the $a_{1g}(\sim 3z^2-r^2)$ level for $K_2ZnF_4:Cu^{2+}$ [19, 22-23]. Furthermore, the optical properties of CuF_6^{4-} complexes in K_2ZnF_4 cannot be *quantitatively* explained considering only the *isolated* CuF_6^{4-} unit at the equilibrium geometry derived for $K_2ZnF_4:Cu^{2+}$ [22, 34]. Nevertheless, in a previous study it was found that both the *d-d* transitions and the unusual ground state of $K_2ZnF_4:Cu^{2+}$ are reasonably explained merely adding in the calculation the internal electric field, $\mathbf{E}_R(\mathbf{r})$, that the rest of ions, belonging to the *tetragonal* lattice, create on the complex where active electrons do reside[22, 34]. These results also imply that due to the action of $\mathbf{E}_R(\mathbf{r})$ there is a gap, Δ_0, between $b_{1g}(\sim x^2-y^2)$ and $a_{1g}(\sim 3z^2-r^2)$ levels of CuF_6^{4-} units in K_2ZnF_4 when the complex is perfectly octahedral[34].

Bearing these facts in mind it is crucial to clarify whether or not the experimental data of d^9 complexes inserted in tetragonal lattices can be understood in the realm of the so called quasi-JT effect. In this framework the JT Hamiltonian is assumed to be the right one with the exception of considering a small gap between the initially degenerate states and keeping the existence of three nearly equivalent distortions[11]. Although the applicability of the quasi-JT effect has been widely assumed, it is however necessary to clarify when such a framework is no longer valid for a quantitative understanding of experimental data.

Seeking to find an answer to this fundamental question we explore in this work the so-called centre I in $Ba_2ZnF_6:Cu^{2+}$ where Cu^{2+} impurities replace Zn^{2+} ions and are also sixfold coordinated[35-36]. Experimental electron paramagnetic resonance (EPR) and electron

nuclear double resonance (ENDOR) results show that the local symmetry around the Cu^{2+} impurity is tetragonal with a principal axis that is *always* coincident with the crystal **c** axis of Ba_2ZnF_6 (Figure 1). Moreover, the experimental g-tensor values, $g_{\parallel} = 1.99$ and $g_{\perp} = 2.36$, measured for the centre I in $Ba_2ZnF_6:Cu^{2+}$ at T = 20 K, undoubtedly prove that the unpaired electron lies in the $a_{1g}(\sim 3z^2\text{-}r^2)$ level[36], a situation which is thus contrary to that observed for d^9 ions in cubic fluorides or chlorides under octahedral coordination[23-33].

Interestingly, although Ba_2ZnF_6 [37] is also a layered perovskite (Figure 1) the octahedron surrounding the Zn^{2+} cation is much more distorted than that corresponding to K_2ZnF_4 which is practically perfect[38]. Calling R_{ax}^0 and R_{eq}^0 the axial and equatorial Zn^{2+}-F^- distances in the host lattice, it turns out that $R_{eq}^0 - R_{ax}^0$ is equal only to 0.3 pm for K_2ZnF_4 [38] while the tetragonal compression is nearly 30 times bigger (i.e. 9 pm) for Ba_2ZnF_6 [37]. Despite this fact the mean value $R_m^0 = (R_{ax}^0 + 2R_{eq}^0)/3$ is found to be identical for both compounds within 0.3% (Table 1). Therefore, this *initial* distortion in the Ba_2ZnF_6 host lattice could help to increase the *final* distortion of the CuF_6^{4-} unit in $Ba_2ZnF_6:Cu^{2+}$ with respect to what is found for $K_2ZnF_4:Cu^{2+}$. For this reason, it is necessary to investigate the experimental splitting, Δ, between the antibonding $b_{1g}(\sim x^2\text{-}y^2)$ and $a_{1g}(\sim 3z^2\text{-}r^2)$ levels measured at the ground state equilibrium geometry of Ba_2ZnF_6. In particular it is crucial to elucidate whether the value $\Delta = 0.80$ eV[35], measured for $Ba_2ZnF_6:Cu^{2+}$ (Table 1) can or not be accounted for just considering the tetragonal distortion undergone by the CuF_6^{4-} complex in the Ba_2ZnF_6 host lattice. Furthermore, it is of fundamental importance to clarify the actual physical reason making the hole in $Ba_2ZnF_6:Cu^{2+}$ to reside in the antibonding $a_{1g}(\sim 3z^2\text{-}r^2)$ level and not in the $b_{1g}(\sim x^2\text{-}y^2)$ one. Both questions imply in a first step to determine the role played by the internal field $\mathbf{E}_R(\mathbf{r})$[17, 22]and thus to know the gap, Δ_0, when the complex is perfectly octahedral[34]. Once this matter is cleared up we explore, in a second step, whether all available data can or not be explained in terms of a quasi-JT effect such as it happens for d^9 ions in a cubic lattice and subject to a strain of $\sim 10^{-3}$ [25, 28, 31].

In summary, in the present study we want to understand why the behavior of Cu^{2+} in the layered perovskites is clearly different from that displayed by d^9 ions in cubic lattices where a static JT effect takes place. For gaining a better insight into this problem the role played by the internal $\mathbf{E}_R(\mathbf{r})$ field for other transition metal impurities[17, 39-40] in insulating compounds is discussed in some detail. This analysis also allows one to assess the reliability of simple models employed in the interpretation of experimental data of insulating compounds containing transition metal cations.

The present work is organized as follows. A short account of employed computational methods is described in the next section while main results obtained in the present work are shown and discussed in the Results and Discussion section together with the condition for having a quasi-JT effect under an internal electric field or an external strain. Moreover, the last part of this section is devoted to provide an ensemble view on the role played by $\mathbf{E}_R(\mathbf{r})$ in insulating compounds containing transition metal cations. Finally,

the general conclusions extracted from the present work are displayed in the last section.

METHODS

Geometry optimizations on periodic supercells simulating diluted Cu^{2+} impurities doped in Ba_2ZnF_6 layered perovskite (tetragonal I4/mmm space group, lattice parameters a = 410.1 pm and c = 1626.3 pm[37], Figure 1) have been performed by means of the CRYSTAL (version 14) code[41] under the framework of the Density Functional Theory (DFT). Calculations were performed using 2x2x1 periodic supercells containing 72 ions. In order to be sure that impurity-impurity interactions between supercells are negligible some calculations were repeated on 3x3x1 supercells and the results were practically unmodified. In the CRYSTAL code, the Bloch wavefunctions are represented by a linear combination of atomic orbitals which, in turn, are expressed as a combination of Gaussian basis functions. All ions have been described by means of basis-sets taken directly from the CRYSTAL's webpage[42]. In particular, we have used all-electron triple-ζ plus polarization (TZP) basis recently developed for Peitinger et al. for Cu, Zn and F and the pseudopotential basis HAYWSC-3111(2d)G_zagorac_2012 for Ba. Following previous works, we have used the B1WC hybrid exchange-correlation functional (including 16% of Hartree-Fock exchange)[43] that has shown to be able to reproduce with great accuracy the geometry and properties of a large number of both pure and doped crystals. The integration in reciprocal space was carried out by sampling the Brillouin zone with the 8x8x4 Monkhorst-Pack net which is enough to provide a full energy convergence.

As the ability of the CRYSTAL program to treat excited states is limited, we have carried out additional geometry optimizations in clusters containing 49 and 109 ions around the Cu^{2+} impurity in both A_{1g} ($b_{1g}^2a_{1g}^1$ configuration) and B_{1g} ($a_{1g}^2b_{1g}^1$) states, and also in the reference state involving the *average* $b_{1g}^{1.5}a_{1g}^{1.5}$ configuration. Calculations have been carried out with the Amsterdam density functional (ADF) code[44], that allows performing DFT calculations on each specific electronic configuration. For this goal we have used the popular B3LYP hybrid functional[45] in the spin-unrestricted Kohn-Sham formalism of the DFT and high-quality all-electron basis sets of triple-ζ plus polarization (TZP) type formed of localized Slater-type functions as implemented in the 2016.101 version of the ADF code[44]. All calculations include the electrostatic $\mathbf{E}_R(\mathbf{r})$ internal field on each computed cluster, that was generated by means of about 200 point charges with values previously fitted to reproduce the electric field corresponding to the infinite system.

Moreover, we have calculated the energies of the *d-d* electronic transitions in CuF_6^{4-} 7 ion clusters in vacuo and also taking into account the electrostatic $\mathbf{E}_R(\mathbf{r})$ field created by the rest of the infinite crystal lattice ions on the cluster. The use of 7 atom clusters for describing the *d-d* transitions of these centers is consistent with the highly localized character of the unpaired electrons residing essentially in the CuF_6^{4-} complex region.

Supporting this view our periodic calculations yield a hole residing less than 2% outside that region.

RESULTS AND DISCUSSION

Equilibrium Geometry and Ground State for CuF_6^{4-} embedded in Ba_2ZnF_6

As there is no experimental information on the actual equilibrium Cu^{2+}-F^- distances for CuF_6^{4-} in Ba_2ZnF_6 [35-36] its calculation is a prerequisite for a further insight into the associated *d-d* transitions, discussed in the next part of this section.

For achieving this goal we have tested in a first step the reliability of the employed methods through the calculation of the lattice parameters *a* and *c*, as well as and the axial, R_{ax}^0, and equatorial, R_{eq}^0, Zn^{2+}-F^- distances corresponding to the pure Ba_2ZnF_6 tetragonal lattice (Figure 1). The comparison between experimental[37] and calculated values is reported on Table 2. It can be noticed that the deviation of values derived through periodic or cluster calculations with respect to experimental ones is smaller than 2%.

In a second step, we have derived, by means of DFT calculations under periodic boundary conditions, the equilibrium geometry and the associated electronic structure corresponding to the centre I in Ba_2ZnF_6:Cu^{2+} involving a CuF_6^{4-} complex (Figure 1). The obtained equilibrium geometry is found to be tetragonal with a C_4 axis *always* parallel to crystal ***c*** axis. The associated electronic structure involves a hole in the $a_{1g}(\sim 3z^2\text{-}r^2)$ level. Both conclusions are in agreement with experimental EPR and ENDOR data[36].

The values of axial, R_{ax}, and equatorial, R_{eq}, Cu^{2+}-F^- distances, corresponding to the CuF_6^{4-} complex embedded in Ba_2ZnF_6 obtained from present calculations are collected in Table 3. When compared to R_{eq}^0 and R_{ax}^0 of the perfect host lattice (Table 1) we see that the $Zn^{2+} \rightarrow Cu^{2+}$ substitution involves a relaxation of ligands, smaller than 4% in all cases. As to the position of nearest ions to the CuF_6^{4-} unit in Ba_2ZnF_6 it is modified by less than 1% with respect to the perfect lattice. In Table 3 the values of R_{ax} and R_{eq} found for Ba_2ZnF_6:Cu^{2+} are also compared to those previously derived[22, 34] for the same unit in K_2ZnF_4. It can be noted that the tetragonal distortion undergone by the CuF_6^{4-} complex in Ba_2ZnF_6 is certainly higher than that obtained for the same complex in K_2ZnF_4. Specifically, the value $R_{eq} - R_{ax}$ = 18.5 pm found in periodic calculations for CuF_6^{4-} in Ba_2ZnF_6 is only 70% higher than the figure calculated for the same unit in K_2ZnF_4 and thus the quantity $R_{eq} - R_{ax}$ does not follow the pattern of $R_{eq}^0 - R_{ax}^0$ corresponding to host lattices (Table 2).

Seeking to investigate whether the behavior of CuF_6^{4-} in Ba_2ZnF_6 follows or not the pattern of a typical JT effect we have calculated the equilibrium geometry for the *average* $b_{1g}^{1.5}a_{1g}^{1.5}$ configuration as well as for the B_{1g} state where the hole is located in the $b_{1g}(\sim x^2\text{-}y^2)$ orbital. As shown in Table 3 the equilibrium geometry found for the average $b_{1g}^{1.5}a_{1g}^{1.5}$ configuration is not octahedral but tetragonally compressed with

$R_{eq}(av)$ = 205.0 pm and $R_{ax}(av)$ = 199.6 pm. This situation is thus different from that found for systems with a static JT effect where $b_{1g}(\sim x^2\text{-}y^2)$ and $a_{1g}(\sim 3z^2\text{-}r^2)$ levels are strictly equivalent and thus the equilibrium geometry for that average configuration is found to be perfectly octahedral[17, 33]. Therefore, the fact that $R_{ax}(av) \neq R_{eq}(av)$ for $Ba_2ZnF_6:Cu^{2+}$ already suggests that $a_{1g}(\sim 3z^2\text{-}r^2)$ and $b_{1g}(\sim x^2\text{-}y^2)$ orbitals are not degenerate when the geometry is perfectly octahedral. A further insight into this matter is given in the next part of this section.

The equilibrium geometry obtained for the B_{1g} state (Table 3) is not consistent with what is expected on the basis of a JT effect. Indeed if for the A_{1g} state the equilibrium geometry corresponds to a compressed situation with R_{eq} - R_{ax} = 15.6 pm one would expect an elongated geometry with R_{ax} - $R_{eq} \approx$ 15 pm for the B_{1g} state[2, 12, 17, 33]. However, the present calculations give only a much reduced value R_{ax} - R_{eq} = 6.4 pm.

For gaining a better insight into this important matter we have also explored the energy dependence of both A_{1g} and B_{1g} states varying the local geometry of the CuF_6^{4-} complex placed in Ba_2ZnF_6. Taking as a departure point the values $R_{ax}(av)$ and $R_{eq}(av)$ derived for the average $b_{1g}^{1.5}a_{1g}^{1.5}$ configuration we have considered the different R_{ax} and R_{eq} values given as a function of the η parameter as follows

$$R_{eq} = R_{eq}(av) \pm \eta \qquad R_{ax} = R_{ax}(av)\ \mu\ 2\eta \tag{1}$$

For the sake of clarity, the results obtained for $Ba_2ZnF_6:Cu^{2+}$ are compared in Figure 2 with those for CuF_6^{4-} in the *cubic* perovskite $KZnF_3$ where a static JT effect takes place. It can be seen that in the latter case the energy curves E(j, η) of j = A_{1g} and B_{1g} states coincide for η = 0. Moreover, if we designates by $E_{min}(j)$ the minimum energy value for such states the condition $E_{min}(j) < E(j, \eta = 0)$ is also fulfilled. Although this behavior may, at first look, resemble a JT effect [33] it is however far from being followed by the curves E(j, η) derived for $Ba_2ZnF_6:Cu^{2+}$ such as it is depicted in Figure 2.

Optical *d-d* transitions for CuF_6^{4-} in Ba_2ZnF_6: role of the internal electric field

Once the tetragonal distortion for CuF_6^{4-} in Ba_2ZnF_6 has been determined it is now crucial to explore whether the experimental *d-d* transitions[35] can be explained considering only the *isolated* CuF_6^{4-} complex at the calculated equilibrium geometry.

The values of three *d-d* transitions derived for the *isolated* CuF_6^{4-} unit when R_{ax} = 188.5 pm and R_{eq} = 207.0 pm are gathered in Table 4 and compared to experimental findings[35]. As shown in Table 4 the calculated energies of $b_{2g}(\sim xy) \rightarrow a_{1g}(\sim 3z^2\text{-}r^2)$ and $b_{1g}(\sim x^2\text{-}y^2) \rightarrow a_{1g}(\sim 3z^2\text{-}r^2)$ transitions are significantly smaller than the corresponding experimental values. In particular the experimental energy gap, Δ = 0.80 eV, between $b_{1g}(\sim x^2\text{-}y^2)$ and $a_{1g}(\sim 3z^2\text{-}r^2)$ orbitals, at the ground state equilibrium geometry, is found to be ~50% higher than the calculated value.

It is worth noting now that for an *isolated* CuF_6^{4-} complex a simple relation between the gap Δ and the distortion parameter R_{eq} - R_{ax} has previously been established[34]

$$\Delta = \beta(R_{eq} - R_{ax}) \qquad (2)$$

where β = 27 meV/pm. Accordingly, if R_{eq} - R_{ax} = 18.5 pm for CuF_6^{4-} in Ba_2ZnF_6 we expect a value Δ = 0.50 eV, a figure which is practically coincident with that calculated for the isolated CuF_6^{4-} complex at the right equilibrium geometry (Table 4) albeit far from the experimental value Δ = 0.80 eV measured by optical absorption for the centre I in Ba_2ZnF_6:Cu^{2+} [36]. This significant discrepancy already points out that the *d-d* transitions measured for CuF_6^{4-} in Ba_2ZnF_6 can hardly be understood just considering the isolated CuF_6^{4-} complex. Indeed, when the electrostatic potential, $V_R(\mathbf{r})$, generating the tetragonal field $\mathbf{E}_R(\mathbf{r})$, is included in the calculation, we see in Table 4 that the three experimental *d-d* transitions are reasonably reproduced. In particular, we notice that the energy of both $b_{2g}(\sim xy) \rightarrow a_{1g}(\sim 3z^2\text{-}r^2)$ and $b_{1g}(\sim x^2\text{-}y^2) \rightarrow a_{1g}(\sim 3z^2\text{-}r^2)$ transitions are raised by about 0.35 eV due to the action of $V_R(\mathbf{r})$ while this electrostatic potential has a smaller effect upon the $e_g(\sim xz,yz) \rightarrow a_{1g}(\sim 3z^2\text{-}r^2)$ transition.

The origin of this relevant result is cleared up looking at the shape displayed by $(-e)V_R(\mathbf{r})$. For the sake of clarity in Figure 3 is depicted the shape of this potential for the cubic perovskite $KZnF_3$ and also for the tetragonal Ba_2ZnF_6 lattice. In Figure 3 is portrayed $V_R(\mathbf{r})$ when the electron coordinate, **r**, moves along the principal tetragonal axis, **c**, or along the **a** axis of Ba_2ZnF_6 while shows that $V_R(\mathbf{r})$ is essentially constant when **r** moves along a principal axis of the cubic $KZnF_3$ perovskite. Nevertheless, in Ba_2ZnF_6, we see that when **r** is varied along <001> and <100> directions, although $\mathbf{E}_R$ = 0 at the copper site, this is no longer true when we go at the ligands position. Specifically, when the unpaired electron is along a <001> direction the $(-e)V_R(\mathbf{r})$ quantity increases its energy while the opposite happens when it lies along the **a** axis. Therefore, as the electronic density in the antibonding $a_{1g}(\sim 3z^2\text{-}r^2)$ level is mainly lying along the **c** axis while in the layer plane for the $b_{1g}(\sim x^2\text{-}y^2)$ orbital the internal field, $\mathbf{E}_R(\mathbf{r})$, contributes to open a gap between the two levels placing $3z^2\text{-}r^2$ above.

These results mean that, in general, there are two contributions to the energy, *E*, of an optical transition corresponding to a transition metal complex embedded in an insulating lattice[46]. In accord with this idea *E* can be written as

$$E = E_{int}(R_{eq}, R_{ax}) + E_{ext} \qquad (3)$$

Here, the first quantity means the intrinsic contribution coming from the *isolated* complex which depends on metal-ligand distances, while the second one, the extrinsic contribution, arises from the effects due to the internal field depending on the position of lattice ions lying outside the complex. Therefore, even if the octahedron surrounding Cu^{2+} is perfect (R_{eq} = R_{ax}), the gap Δ_0 is *not necessarily* equal to zero due to the existence of the extrinsic contribution, Δ_{ext}, which can be different from zero for a *non-cubic* host

lattice[34]. From data gathered in Table 4, it can be inferred $\Delta_0 = \Delta_{ext} = 0.35$ eV for CuF_6^{4-} in Ba_2ZnF_6, a quantity similar to that previously found for $K_2ZnF_4:Cu^{2+}$ [22, 34].

This result also allows one to understand the actual origin of the anomalous ground state of $Ba_2ZnF_6:Cu^{2+}$ when compared to that found for d^9 ions in cubic fluorides or chlorides under octahedral coordination[23-33]. Indeed if when $R_{eq} = R_{ax}$ the $a_{1g}(\sim 3z^2\text{-}r^2)$ level lies ~0.35 eV *above* $b_{1g}(\sim x^2\text{-}y^2)$ due to the action of $\mathbf{E}_R(\mathbf{r})$, this fact already forces the hole to be located in the $a_{1g}(\sim 3z^2\text{-}r^2)$ level. Once the ground state of CuF_6^{4-} in Ba_2ZnF_6 involves a *positive* hole in the axial $a_{1g}(\sim 3z^2\text{-}r^2)$ it induces a reduction of the axial metal-ligand distance, R_{ax}. Moreover, this reduction is also favoured by the substantial *increase* of $(-e)V_R(\mathbf{r})$ for Ba_2ZnF_6 when $\mathbf{r}$ is along the [001] direction (Figure 3). These facts are thus the actual physical reason behind the unusual compressed equilibrium geometry found in $Ba_2ZnF_6:Cu^{2+}$. The rapid increase of $(-e)V_R(\mathbf{r})$ along the [001] direction (Figure 3) also explains, albeit qualitatively, why the equilibrium geometry for the $b_{1g}^{1.5}a_{1g}^{1.5}$ configuration is found to be slightly compressed or why the equilibrium $|R_{eq} - R_{ax}|$ value for the A_{1g} state is 2.5 times higher than that found for the B_{1g} state (Table 3). All these results, ultimately due to the existence of $\mathbf{E}_R(\mathbf{r})$, point out that the properties displayed by $Ba_2ZnF_6:Cu^{2+}$ cannot be understood in a pure JT framework. A similar situation holds for CuF_6^{4-} in the tetragonal K_2ZnF_4 lattice[22, 34].

It is worth noting now that other characteristics of the JT effect have been shown not to be fulfilled by experimental and theoretical results on Cu^{2+} in a tetragonal lattice. For instance, while in a system displaying an $E\otimes e$ JT effect the *e* vibration mode is degenerate this degeneracy has been shown to be clearly broken for CuF_6^{4-} in the tetragonal perovskite K_2ZnF_4 [22].

d^9 ions in cubic and layered lattices: macroscopic differences

Let us now focus on the *macroscopic* differences between the behaviour of Cu^{2+} in layered perovskites and in cubic crystals where in all cases the impurity is sixfold coordinated. When a MX_6 complex ($M = Cu^{2+}, Ag^{2+}, Ni^{+}$; $X = F^{-}, Cl^{-}$) is embedded in cubic lattices, like $KZnF_3$, $CsCdF_3$ or NaCl, a static JT effect is observed[23-29, 32] whose main fingerprints are the following: (a) At low temperatures *three* centers with tetragonal symmetry are *simultaneously* observed by EPR. Although such centers are physically equivalent they differ in the orientation of its principal axis which is just one of the three C_4 axes of the cubic crystal. (b) In all cases, at equilibrium, the unpaired electron is lying in the $b_{1g}(\sim x^2\text{-}y^2)$ orbital and the ligand octahedron is elongated. (c) When temperature is raised the EPR spectrum becomes isotropic. The temperature of this transition, T_t, has been found to lie in the region 30-200 K working in the X band. For instance, $T_t \approx 30$ K for Cu^{2+}-doped $CsCdF_3$ or $KZnF_3$ [24-25] while $T_t = 160$ K for $KCl:Ag^{2+}$ [29]. (d) The gap, Δ, observed at equilibrium is explained exclusively in terms of the local distortion described by the actual R_{eq} and R_{ax} values. A detailed study on this matter has been carried out for $KCl:Ag^{2+}$ [33].

The preceding characteristics of a static JT effect for Cu^{2+}, Ag^{2+} or Ni^{+} in cubic fluorides or chlorides are not followed by data for CuF_6^{4-} in layered perovskites like Ba_2ZnF_6 or K_2ZnF_4. Main arguments supporting this assertion are: (a) All CuF_6^{4-} complexes formed in the tetragonal host lattices are found to have the *same* principal axis, the **c** axis of the host crystal, and thus there are not three magnetically non-equivalent centres at low temperatures[19, 23, 36, 47]. (b) The hole in layered perovskites is surprisingly placed in the $a_{1g}(\sim 3z^2\text{-}r^2)$ level and not in $b_{1g}(\sim x^2\text{-}y^2)$. (c) The EPR spectrum of both $K_2ZnF_4:Cu^{2+}$ [47] and $Ba_2ZnF_6:Cu^{2+}$ [36] has been shown to display a tetragonal symmetry in the *whole* temperature range 4-300 K. (d) While for a MX_6 complex ($M = Cu^{2+}$, Ag^{2+}, Ni^{+}; $X = F^{-}$, Cl^{-}) in a cubic lattice the extrinsic contribution to the gap, Δ_{ext}, is necessarily equal to zero this is no longer true when we deal with a host lattice with tetragonal symmetry.

Absence of a quasi Jahn-Teller effect in $Ba_2ZnF_6:Cu^{2+}$ due to $E_R(r)$

The preceding sections have shown that the properties of CuF_6^{4-} units in Ba_2ZnF_6 are not understandable in terms of a static JT effect mainly due to the existence of an internal electric field $\mathbf{E}_R(\mathbf{r})$ displaying tetragonal symmetry. For this reason, it is now necessary to explore under what conditions the *addition* of an internal field of lower symmetry does not significantly modify the pattern characteristic of a static JT system[2, 12]. In other words, we need to understand why an extrinsic contribution Δ_{ext} of *only* 0.35 eV prevents the existence of a quasi-JT effect for $Ba_2ZnF_6:Cu^{2+}$.

For achieving this goal let us firstly consider the case of a MX_6 complex ($M = Cu^{2+}$, Ag^{2+}; $X = F^{-}$, Cl^{-}) placed in a cubic lattice and displaying a static JT effect. Under these circumstances, $\Delta_{ext} = 0$ and also $\Delta E_{int}(R_{eq}, R_{ax}) = 0$ when $R_{eq} = R_{ax}$ (Figure 2). These facts just reflect that when the ligand octahedron is perfect the $a_{1g}(\sim 3z^2\text{-}r^2)$ and $b_{1g}(\sim x^2\text{-}y^2)$ levels are degenerate. Nevertheless, if we place the positive hole in the $b_{1g}(\sim x^2\text{-}y^2)$ level it forces an equilibrium geometry such as $R_{ax} > R_{eq}$ [17, 48] and involves a relaxation energy termed $E_{JT}(B_{1g})$ (Figure 2). Similarly, if the hole is now located in the a_{1g} $(\sim 3z^2\text{-}r^2)$ level then $R_{ax} < R_{eq}$ at equilibrium and there is an associated relaxation energy $E_{JT}(A_{1g})$ which is not exactly equal to $E_{JT}(B_{1g})$ (Figure 2). For all explored MX_6 complexes ($M = Cu^{2+}$, Ag^{2+}, Ni^{+}; $X = F^{-}$, Cl^{-}) placed in a cubic lattice, displaying a static JT effect, it turns out that the energy gain $E_{JT}(B_{1g})$ is found to be somewhat higher than $E_{JT}(A_{1g})$[30, 33-34]. Thus, these systems exhibit an electronic ground state with a hole placed in the $b_{1g}(\sim x^2\text{-}y^2)$ level[23-29, 31].

According to this reasoning the quantity $B = E_{JT}(B_{1g}) - E_{JT}(A_{1g})$ (Figure 2) has a fundamental role in the realm of the JT effect. Indeed, *B* not only measures the gap between the ground and first excited state computed at the corresponding equilibrium geometry but it is also the energy barrier among physically equivalent distortions[2, 12]. The actual value of this key quantity for different JT systems has been investigated in recent years[12, 18, 30, 33-34].

Let us now consider the effects of adding an internal electric field of tetragonal symmetry, $\mathbf{E}_R(\mathbf{r})$, on the electronic ground state of a given JT complex. As we have seen the internal field, $\mathbf{E}_R(\mathbf{r})$, produces a different energy shift, $\varepsilon_T(x^2-y^2)$ and $\varepsilon_T(3z^2-r^2)$, on the $b_{1g}(\sim x^2-y^2)$ and $a_{1g}(\sim 3z^2-r^2)$ levels *even if* $R_{eq} = R_{ax}$. In other words, the extrinsic contribution to the gap between these two levels, Δ_{ext}, is just given by

$$\Delta_{ext} = \varepsilon_T(3z^2-r^2) - \varepsilon_T(x^2-y^2) \qquad (4)$$

According to the present reasoning, if in a d^9 JT system the hole lies in the $b_{1g}(\sim x^2-y^2)$ level and thus the ligand octahedron is elongated, the *addition* of $\mathbf{E}_R(\mathbf{r})$ can change the nature of the electronic ground state as well as the existence of three quasi equivalent distortions. The non-existence of this change is thus favored by the condition

$$\Delta_{ext} < B \qquad (5)$$

Results on several elongated systems displaying a static JT effect show that the barrier is lying in the 6-150 meV range[12, 18, 30, 33-34]. More precisely, typical values for this magnitude are found for $KZnF_3:Cu^{2+}$ and $NaCl:Ag^{2+}$ being, respectively, B = 8 and 62 meV, while the largest one we are aware corresponds to B = 127 meV for $KCl:Ag^{2+}$ [12, 18, 30, 34].

The scale of these values is a factor 3-50 smaller than the gap created between $b_{1g}(\sim x^2-y^2)$ and $a_{1g}(\sim 3z^2-r^2)$ levels by the internal field in $Ba_2ZnF_6:Cu^{2+}$ giving rise to Δ_{ext} = 0.35 eV. In particular, this extrinsic contribution is about 40 times higher than the value B = 8 meV derived for the JT system $KZnF_3:Cu^{2+}$ (Figure 2). Thus, according to this simple reasoning, the extrinsic contribution Δ_{ext} = 0.35 eV found in $Ba_2ZnF_6:Cu^{2+}$ largely suffices for drastically changing the JT pattern such it has been shown in the previous parts of this section. For this reason, an explanation of properties observed in $Ba_2ZnF_6:Cu^{2+}$ on the basis of a quasi-JT effect has to be ruled out. In particular, the ground state of $Ba_2ZnF_6:Cu^{2+}$, involving a hole in the $a_{1g}(\sim 3z^2-r^2)$ level, is different from that observed for d^9 ions in perfect cubic fluoride or chloride lattices where the hole is located in the $b_{1g}(\sim x^2-y^2)$ orbital. As we have proved, this relevant difference is mainly due to the action of the anisotropic internal field $\mathbf{E}_R(\mathbf{r})$ in the layered perovskite and not to the JT effect.

Although for all MX_6 complexes ($M = Cu^{2+}, Ag^{2+}, Ni^{+}$) in fluoride or chloride cubic lattices explored up to now the hole is found in the $b_{1g}(\sim x^2-y^2)$ level and the ligand octahedron elongated this is *not necessarily* true for every system displaying a static JT effect. Indeed it has recently been demonstrated that Ni^+ in the cubic CaO lattice exhibits a static JT effect with a hole in the $a_{1g}(\sim 3z^2-r^2)$ level and a compressed geometry[49]. The main factors favoring the compressed geometry in a static JT system are discussed in Refs.[17, 33, 49].

Applied strains on d^9 ions in a cubic lattice: limits for a quasi-Jahn-Teller effect

In this section we explore the effects of an applied uniaxial strain on a system *initially* displaying a static JT effect. The main objective is to determine the conditions for observing experimentally a quasi-JT effect when the strain is varied.

For the sake of clarity let us consider a d^9 ion in a cubic lattice displaying an elongated geometry ($R_{ax} > R_{eq}$) and a hole in $b_{1g}(\sim x^2-y^2)$, being OZ the principal axis. If the system is subject to a strain, described by a strain tensor whose only non-zero component is e_{zz}, this tetragonal perturbation induces shifts, termed $\varepsilon_S(3z^2-r^2)$ and $\varepsilon_S(x^2-y^2)$, on the two considered *d*-levels. If $e_{zz} < 0$ then $\varepsilon_S(3z^2-r^2) > \varepsilon_S(x^2-y^2)$. Thus, similarly to Eq. (5), the condition favoring not to modify the ground state under the applied strain is just given by

$$\varepsilon_S(3z^2-r^2) - \varepsilon_S(x^2-y^2) < B \qquad (6)$$

For a JT system the quantity $\varepsilon_S(3z^2-r^2) - \varepsilon_S(x^2-y^2)$ is expressed in terms of the e_{zz} strain as follows[2, 12, 28]

$$\varepsilon_S(3z^2-r^2) - \varepsilon_S(x^2-y^2) = (3/2)V_2 e_{zz} \qquad (7)$$

where in turn V_2 can be expressed in terms of the linear vibronic coupling constant, V_{1e},

$$V_2 = -(2/\sqrt{3})V_{1e}R_{av}e_{zz} \qquad (8)$$

Eqs. (6-8) just mean that if $V_{1e} \sim 1$ eV/Å and $R_{av} \sim 2.5$ Å then a quasi-JT effect should be observed for $e_{zz} < 10^{-2}$ in the case of a barrier B = 60 meV.

EPR experiments performed for NaCl:Cu^{2+} at T = 77 K involving strains up to $\sim 3\times10^{-3}$ [28]prove the existence of a quasi-JT regime. In the absence of an external strain there are three *equally* populated centres whose C_4 axis is parallel to the X, Y or Z axis of the crystal because the ground state energy of such centres, E_I (I = X, Y, Z) is the same[12, 28]. Although this degeneracy is broken by the action of the applied strain the EPR spectra are however close to those observed for e_{zz} = 0 characteristic of a JT effect. The similarities and differences with respect to e_{zz} = 0 are the following[28]: (1) For a general orientation of the applied magnetic field, **H**, the signals from the three distortions with the C_4 axis parallel to the X, Y or Z axes are *all* observed in EPR spectra. (2) The values of the EPR parameters corresponding to each centre are essentially those measured at zero-strain as they are practically insensitive to applied strains smaller than $\sim 10^{-2}$ [50]. (3) Nevertheless, the population of the three centers is now different as E_Z is no longer equal to E_X or E_Y due to the action of the applied strain.

Under an external strain, $e_{zz} < 0$, the difference between E_Z and E_X or E_Y is simply given by[2, 12]

$$E_Z - E_X = (3/2)V_2 e_{zz} \qquad (9)$$

Thus, if $e_{zz} \sim -3\times10^{-3}$ and $V_2 \sim -2$ eV/strain then $E_Z - E_X \sim 10$ meV. As this quantity is comparable to kT = 7meV if T = 77 K, this explains that the three centres with the C_4 axis

parallel to the X, Y, Z axes in NaCl:Cu^{2+} are still observed under a $e_{zz} \sim 3\times10^{-3}$ strain although with a *different* intensity[28]. A quasi-JT regime has also been observed for $CsCdF_3$:Cu^{2+} and NaF:Ag^{2+} under an applied uniaxial stress[24-25, 31].

The present discussion on the quasi-JT effect points out that the ground state of a system displaying a static JT effect can be modified when subject to a e_{zz} strain. This means that if the d^9 JT complex is elongated with a principal axis parallel to OZ axis then both the ground state and the equilibrium geometry can be changed under an axial $e_{zz} < 0$ strain, especially if the barrier, B, is low. Preliminary calculations carried out on $KZnF_3$:Cu^{2+}, where B is only equal to 8 meV, supports that such a change can be reached for $e_{zz} \sim 5\times10^{-3}$.

It is worth noting now that in any *real* crystal there are random strains produced by the unavoidable presence of dislocation and point defects. Such random strains destroy the equivalence of three adiabatic distortions which appear in a $E\otimes e$ JT system being thus responsible for the observation of a static JT effect at low temperatures[2, 12, 49]. Nevertheless, as in the case of random strains $|e_{zz}|$ is of the order of 10^{-4} the associated perturbation cannot alter the nature of the ground state in a static JT effect.

Extrinsic and intrinsic contributions: a general view

The present results prove the important role played by the internal field $\mathbf{E}_R(\mathbf{r})$ for a correct understanding of the *anomalous* ground state observed for Ba_2ZnF_6:Cu^{2+} as well as its associated *d-d* transitions. Indeed, simply looking at the shape of $V_R(\mathbf{r})$ (Figure 3) we realize that it opens a gap between the two $b_{1g}(\sim x^2-y^2)$ and $a_{1g}(\sim 3z^2-r^2)$ levels even if the CuF_6^{4-} complex is perfectly octahedral. Moreover, this gap mainly comes from the electronic density lying in the ligand region rather than close to the copper site where $\mathbf{E}_R(\mathbf{0}) = 0$.

Obviously, the internal electric field has to play a relevant role for other transition metal impurities placed in layered insulators. A direct proof of this assertion appears looking at the properties displayed by the CrF_6^{3-} complex placed in the tetragonal K_2MgF_4 lattice with remote charge compensation[51]. Both the experimental g-tensor ($g_{\|} = 1.9727$, $g_{\perp} = 1.9743$) and the existence of a zero-field splitting ($D = 0.042$ cm^{-1}) observed in EPR spectra[51] support a clear tetragonal point symmetry for this center although the calculated R_{eq} and R_{ax} values are *identical* within 0.3% [52]. Again the observed tetragonal symmetry in EPR spectra has been shown to arise from the effects of $\mathbf{E}_R(\mathbf{r})$ that induces a gap between $b_{1g}(\sim x^2-y^2)$ and $a_{1g}(\sim 3z^2-r^2)$ levels leading to a splitting of 120 meV in the $^4T_2$ first excited state[52].

According to the present analysis the internal electric field, although often ignored, cannot be discarded in any right understanding of spectroscopic properties due to transition metal ions in insulating lattices. So, $\mathbf{E}_R(\mathbf{r})$, aside from being responsible for the different color in ruby (Al_2O_3:Cr^{3+}), emerald ($Be_3Al_2Si_6O_{18}$:Cr^{3+}) and alexandrite

($BeAl_2O_4:Cr^{3+}$) [39], can also influence the gap, 10Dq, between $t_{2g}(xz, yz, xy)$ and $e_g(x^2-y^2, 3z^2-r^2)$ levels of perfect octahedral CrO_6^{9-}complexes embedded in cubic lattices[46]. In other words, similarly to Eq. (3) we can write for these cases

$$10Dq = 10Dq_{int}(R) + 10Dq_{ext} \quad (10)$$

where the intrinsic contribution $10Dq_{int}(R)$ is sensitive to the actual value of the metal-ligand distance, R.

The existence of an extrinsic contribution for $LiBaF_3$ [40], displaying a cubic inverted perovskite structure, explains why MF_6^{4-} complexes (M = Mn, Ni, Co) exhibit a 10Dq value which is systematically ~0.2 eV higher[53] when embedded in that lattice than in the normal perovskite $KMgF_3$ [17]. In the same vein, the identical 10Dq = 2 eV measured for $MgO:Cr^{3+}$ [54]and the emerald[55-56] has been shown to come from an extrinsic contribution $10Dq_{ext}$ = 0.2 eV for the former system while it is practically null for emerald[46].

When in the cubic MgO lattice the host cation Mg^{2+} is replaced by a transition metal impurity like Cr^{3+}, with remote charge compensation, the lattice symmetry implies that the internal electric field at the metal cation is zero. This situation, somewhat similar to that previously discussed for $Ba_2ZnF_6:Cu^{2+}$, stresses that the effects of $\mathbf{E}_R(\mathbf{r})$ upon the observed spectroscopic properties cannot be understood neglecting the electronic density present in the ligand region.

Furthermore, the actual value of the intrinsic contribution, $10Dq_{int}(R)$, as well as its dependence upon the metal-ligand distance, R, have been shown to arise from the different covalent bonding in the antibonding $t_2(xz, yz, xy)$ and $e(x^2-y^2, 3z^2-r^2)$ levels of an octahedral or tetrahedral complex[57]. Along this line for complexes like MnF_6^{4-}, CrF_6^{3-} or FeO_4^{2-} $10Dq_{int}(R)$ depends on R^{-n} ($n \approx 5$) and this strong dependence has been shown to come mainly from the hybridization of 3d(e) levels with 2s ligand levels[17, 58]. Although the rough crystal-field theory, which treats the ligands as point charges, predicts a dependence of $10Dq_{int}(R) \propto R^{-5}$ this agreement has to be viewed only as a fortuitous coincidence because that theory also leads to 10Dq values which are *one order of magnitude* smaller than experimental ones[17]. For this reason, although there are still papers claiming that an experimental dependence $10Dq \propto R^{-n}$ ($n \approx 5$) proves the validity of crystal-field theory[59] that assertion is simply meaningless.

Bearing in mind that electron localization is a fingerprint of insulating materials[60-61] it can be expected that the internal electric field also plays a relevant role for understanding the ground state of *pure* insulating compounds. Along this line it has been shown that in La_2CuO_4 $\mathbf{E}_R(\mathbf{r})$ forces the hole to be in the x^2-y^2 while in K_2CuF_4 the unpaired electron lies in an orbital with a dominant $3z^2-r^2$ character as a result of the internal electric field[62]. Other examples showing the importance of the internal field, $\mathbf{E}_R(\mathbf{r})$, for understanding the orbital ordering in pure non-cubic transition metal compounds are given in Ref.[62].

CONCLUSIONS

The present results prove the absence of symmetry breaking for CuF_6^{4-} in Ba_2ZnF_6 as even when $R_{ax} = R_{eq}$ the complex *already* exhibits a D_{4h} symmetry due to the presence of the anisotropic internal field, $\mathbf{E}_R(\mathbf{r})$. Furthermore, they also demonstrate that $\mathbf{E}_R(\mathbf{r})$ in Ba_2ZnF_6, leading to $\Delta_{ext} \sim 0.35$ eV, can destroy the pattern characteristic of a JT effect. This means that, contrary to what is found for systems like $NaCl:Cu^{2+}$ or $CsCdF_3:Cu^{2+}$ under $e_{zz} \sim 10^{-3}$ strains, we cannot understand the properties displayed by CuF_6^{4-} in the tetragonal lattices Ba_2ZnF_6 or K_2ZnF_4 on the basis of a quasi-JT effect.

The structural and electronic properties of compounds containing d^9 ions are very often discussed *assuming* the existence of a JT effect. The present results stress however, that if the host lattice is not cubic that assumption may, in general, not to be right. The construction of correct models on these systems necessarily involves fully assuming the low-symmetry of the system, including changes in the splitting of the levels, forces, frequencies, etc. that are not present in a JT model and that are closely related to the internal field $\mathbf{E}_R(\mathbf{r})$. Moreover, the appearance of the three minima typically associated to a JT problem now involves the vibronic coupling between non-degenerate levels and thus if orthorhombic minima were present, which is not assured, it could only be explained through the use of a full pseudo Jahn-Teller model.[6, 63-65]

At the time of publication we found a recent paper[66] claiming that the properties of $K_2ZnF_4:Cu^{2+}$ can be explained on the basis of the JT effect in the same way as $KZnF_3:Cu^{2+}$. This assertion is supported in Ref. [66] indicating that the absolute value of the experimental splitting between $b_{1g}(\sim x^2-y^2)$ and $a_{1g}(\sim 3z^2-r^2)$ levels in $KZnF_3:Cu^{2+}$ ($|\Delta| = 0.62$ eV) is nearly identical to that for $K_2ZnF_4:Cu^{2+}$($|\Delta| = 0.64$ eV). However, the later statement raises questions at various levels: (1) As it was previously explained, $K_2ZnF_4:Cu^{2+}$ [47] and $Ba_2ZnF_6:Cu^{2+}$ [36] can not be considered as JT systems because their experimental EPR data do not exhibit the characteristic fingerprint of a static JT system that is, however, well observed for $KZnF_3:Cu^{2+}$ [25]. (2) As the character of the ground state in both systems is different, Δ is positive for $K_2ZnF_4:Cu^{2+}$ and $Ba_2ZnF_6:Cu^{2+}$ (Table 1) but negative[23, 25] for $KZnF_3:Cu^{2+}$ (see also Figure 2). This key fact is not explained in Ref. [66] while its actual origin is well understood through the present work. (3) The value $|\Delta| = 0.62$ eV considered in Ref. [66] for $KZnF_3:Cu^{2+}$ does not correspond to any experimental measurement. In this respect, optical absorption data on $KZnF_3:Cu^{2+}$ show[21, 23] that no absorption occurs in the range 0.5-0.94 eV after which the $e_g(xz;yz) \rightarrow b_{1g}(x^2-y^2)$ transition is observed. Moreover, first-principle calculations[34] match all observed bands[23] and are consistent with this fact since they predict $\Delta = -0.40$ eV, well below the value $|\Delta| = 0.62$ eV given in Ref. [66].

The study carried out in this work shows the importance of the internal field $\mathbf{E}_R(\mathbf{r})$ for a *quantitative* understanding of spectroscopic properties displayed by transition metal cations in insulating lattices. This implies that models which try to explain such

properties based solely on isolated complexes are, in general, not correct[17, 34, 39, 52]. For this reason, in the interpretation of experimental data, the use of a simple model should be avoided unless all its assumptions are well justified. In this regard first principle calculations have shown to be a valuable tool to check the validity of simple model's assumptions.

It is worth noting now that $\mathbf{E}_R(\mathbf{r})$ is actually determined by a few shells of ions *lying close* to the considered complex as further ions lead to a potential $V_R(\mathbf{r})$ essentially flat in the complex region where active electrons reside. The contribution of different shells of ions to the total $V_R(\mathbf{r})$ potential has been explored for systems like ruby[67], MgO:Cr^{3+} [46] or $LiBaF_3$:Mn^{2+} [40].

We have seen in the present work that the internal electric field induces an extrinsic contribution, Δ_{ext}, to the $a_{1g}(\sim 3z^2\text{-}r^2)$ - $b_{1g}(\sim x^2\text{-}y^2)$ gap of Ba_2ZnF_6:Cu^{2+} of only ~0.35 eV. Nevertheless, very recently it has been proved that for the square-planar CuO_4^{6-} complex formed in $CaCuSi_4O_{10}$[68] the internal electric field produces even higher shifts (Δ_{ext} ~1 eV)[69], a crucial fact which is behind the blue color displayed by the Egyptian Blue pigment. According to this result it could be expected that, in comparison to what is found for CuF_6^{4-} in Ba_2ZnF_6:Cu^{2+}, higher extrinsic contributions also appear in the case of square-planar CuF_4^{2-} complexes formed in fluoride lattices[35, 70]. Work along this line is now underway.

Acknowledgments

The support by the Spanish Ministerio de Ciencia y Tecnología under Projects FIS2012-30996 and FIS2015-64886-C5-2-P is acknowledged.

References

1. Jahn, H. A.; Teller, E., Stability of Polyatomic Molecules in Degenerate Electronic States. I. Orbital Degeneracy. *Proc. R. Soc. London, Ser. A* **1937,** *161*, 220-235.
2. Ham, F. S., Jahn-Teller Effects in EPR spectra. In *Electron Paramagnetic Resonance*, Geschwind, S., Ed. Plenum: New York, 1972.
3. Murphy, B.; Hathaway, B., The Stereochemistry of the Copper(II) Ion in the Solid-State - Some Recent Perspectives Linking the Jahn-Teller Effect, Vibronic Coupling, Structure Correlation Analysis, Structural Pathways and Comparative X-Ray Crystallography. *Coord. Chem. Rev.* **2003,** *243*, 237-262.
4. Tretyakov, Y. D.; Goodilin, E. A., Fundamental Chemical Features of Complex Manganites and Cuprates for Advanced Functional Materials Engineering. *Pure Appl. Chem.* **2004,** *76*, 1749-1768.
5. McLain, S. E.; Dolgos, M. R.; Tennant, D. A.; Turner, J. F. C.; Barnes, T.; Proffen, T.; Sales, B. C.; Bewley, R. I., Magnetic Behaviour of Layered Ag(II) Fluorides. *Nat. Mater.* **2006,** *5*, 561-566.
6. Bersuker, I. B., *The Jahn-Teller Effect*. Cambridge University Press: 2006.

7. Keller, H.; Bussmann-Holder, A.; Muller, K. A., Jahn-Teller Physics and High-T-c Superconductivity. *Mater. Today* **2008,** *11*, 38-46.
8. Tsujimoto, Y.; Yamaura, K.; Takayama-Muromachi, E., Oxyfluoride Chemistry of Layered Perovskite Compounds. *Appl. Sci.* **2012,** *2*, 206-219.
9. Halcrow, M. A., Jahn-Teller Distortions in Transition Metal Compounds, and their Importance in Functional Molecular and Inorganic Materials. *Chem. Soc. Rev.* **2013,** *42*, 1784-1795.
10. Kurzydlowski, D.; Derzsi, M.; Mazej, Z.; Grochala, W., Crystal, Electronic, and Magnetic Structures of M_2AgF_4 (M = Na-Cs) Phases as Viewed from the DFT plus U Method. *Dalton Trans.* **2016,** *45*, 16255-16261.
11. Reinen, D., The Modulation of Jahn-Teller Coupling by Elastic and Binding Strain Perturbations-A Novel View on an Old Phenomenon and Examples from Solid-State Chemistry. *Inorg. Chem.* **2012,** *51*, 4458-4472.
12. Garcia-Fernandez, P.; Trueba, A.; Barriuso, M. T.; Aramburu, J. A.; Moreno, M., Dynamic and Static Jahn-Teller Effect in Impurities: Determination of the Tunneling Splitting. In *Vibronic Interactions and the Jahn-Teller Effect: Theory and Applications*, Atanasov, M.; Daul, C.; TregennaPiggott, P. L. W., Eds. 2012; Vol. 23, pp 105-142.
13. Laredo, E.; Paul, W. B.; Rowan, L.; Slifkin, L., Interactions between Self-Trapping and Solute Trapping of Photocarriers in Pd-Doped AgCl. *Phys. Rev. B* **1983,** *27*, 2470-2476.
14. Bennebroek, M. T. Ph.D. Thesis: High-Field Electron Nuclear Double Resonance Spectroscopy on Photo-Induced Centers in Silver Halides. University of Leiden, 1996.
15. Loftager, S.; Garcia-Fernandez, P.; Aramburu, J. A.; Moreno, M.; Garcia-Lastra, J. M., Stability and Polaronic Motion of Self-Trapped Holes in Silver Halides: Insight through DFT plus U Calculations. *J. Phys. Chem. C* **2016,** *120*, 8509-8524.
16. Bill, H., Observation of the Jahn-Teller Effect with Electron Paramagnetic Resonance. In *The Dynamical Jahn-Teller Effect in Localized Systems*, Perlin, Y. E.; Wagner, M., Eds. Elsevier: Amsterdam, 1984.
17. Moreno, M.; Barriuso, M. T.; Aramburu, J. A.; Garcia-Fernandez, P.; Garcia-Lastra, J. M., Microscopic Insight into Properties and Electronic Instabilities of Impurities in Cubic and Lower Symmetry Insulators: the Influence of Pressure. *J. Phys.: Condens. Matter* **2006,** *18*, R315-R360.
18. Garcia-Fernandez, P.; Trueba, A.; Barriuso, M. T.; Aramburu, J. A.; Moreno, M., Tunneling Splitting of Jahn-Teller Ions in Oxides. *Phys. Rev. Lett.* **2010,** *104*, 035901
19. Riley, M. J.; Dubicki, L.; Moran, G.; Krausz, E. R.; Yamada, I., Absorption and Magnetic Circular-Dichroism Spectra of the Compressed Copper(II) Ion in K_2ZnF_4. *Chem. Phys.* **1990,** *145*, 363-373.
20. Garcia-Lastra, J. M.; Aramburu, J. A.; Barriuso, M. T.; Moreno, M., Impurities in Noncubic Crystals: Stabilization Mechanisms for Jahn-Teller Ions in Layered Perovskites. *Phys. Rev. Lett.* **2004,** *93*, 226402
21. Riley, M. J., Geometric and Electronic Information from the Spectroscopy of Six-Coordinate Copper(II) Compounds. *Top. Curr. Chem.* **2001,** *214*, 57-80.
22. Aramburu, J. A.; Garcia-Lastra, J. M.; Garcia-Fernandez, P.; Barriuso, M. T.; Moreno, M., Cu^{2+} in Layered Compounds: Origin of the Compressed Geometry in the Model System $K_2ZnF_4:Cu^{2+}$. *Inorg. Chem.* **2013,** *52*, 6923-6933.
23. Dubicki, L.; Riley, M. J.; Krausz, E. R., Electronic-Structure of the Copper(II) Ion Doped in Cubic $KZnF_3$. *J. Chem. Phys.* **1994,** *101*, 1930-1938.

24. Minner, E.; Lovy, D.; Bill, H., Electron-Paramagnetic-Resonance and Relaxation Study of Copper(II) and Silver(II) In $CsCdF_3$ Single-Crystals. *J. Chem. Phys.* **1993,** *99*, 6378-6383.
25. Minner, E. M. C. Ph.D. Thesis: Etude Spectroscopique des Ions Jahn-Teller Cuivre et Argent Bivalents dans des Monocristaux de Fluoroperovskites de Composition Chimique AMF_3. University of Geneva, 1993.
26. Villacampa, B.; Alcala, R.; Alonso, P. J.; Moreno, M.; Barriuso, M. T.; Aramburu, J. A., EPR Study of Ni^+ Centers in $CsCaF_3$. *Phys. Rev. B* **1994,** *49*, 1039-1047.
27. Zorita, E.; Alonso, P. J.; Alcala, R., Tetragonal Ni^+ Ions in X-Ray-Irradiated $KMgF_3$-Ni. *Phys. Rev. B* **1987,** *35*, 3116-3121.
28. Borcherts, R. H.; Kanzaki, H.; Abe, H., EPR Spectrum of a Jahn-Teller System, NaCl-Cu^{2+}. *Phys. Rev. B* **1970,** *2*, 23-+.
29. Sierro, J., Paramagnetic Resonance of the Ag^{2+} Ion in Irradiated Alkali Chlorides. *J. Phys. Chem. Solids* **1967,** *28*, 417-422.
30. Trueba, A.; Garcia-Lastra, J. M.; de Graaf, C.; Garcia-Fernandez, P.; Barriuso, M. T.; Aramburu, J. A.; Moreno, M., Jahn-Teller Effect in Ag^{2+} Doped KCl and NaCl: Is There any Influence of the Host Lattice? *Chem. Phys. Lett.* **2006,** *430*, 51-55.
31. Monnier, A.; Gerber, A.; Bill, H., The Jahn-Teller System Ag^{2+}-NaF, an Electron-Paramagnetic Resonance and Optical-Absorption Study. *J. Chem. Phys.* **1991,** *94*, 5891-5896.
32. Shengelaya, A.; Drulis, H.; Macalik, B.; Suszynska, M., Low Temperature ESR Spectra of Nickel-Doped NaCl Crystals. *Z. Phys. B: Condens. Matter* **1996,** *101*, 373-376.
33. Barriuso, M. T.; Ortiz-Sevilla, B.; Aramburu, J. A.; Garcia-Fernandez, P.; Garcia-Lastra, J. M.; Moreno, M., Origin of Small Barriers in Jahn-Teller Systems: Quantifying the Role of 3d-4s Hybridization in the Model System NaCl:Ni^+. *Inorg. Chem.* **2013,** *52*, 9338-9348.
34. Garcia-Fernandez, P.; Teresa Barriuso, M.; Garcia-Lastra, J. M.; Moreno, M.; Antonio Aramburu, J., Compounds Containing Tetragonal Cu^{2+} Complexes: Is the d_{x2-y2}-d_{3z2-r2} Gap a Direct Reflection of the Distortion? *J. Phys. Chem. Lett.* **2013,** *4*, 2385-2390.
35. Reinen, D.; Steffen, G.; Hitchman, M. A.; Stratemeier, H.; Dubicki, L.; Krausz, E. R.; Riley, M. J.; Mathies, H. E.; Recker, K.; Wallrafen, F., The Optical-Spectrum of Ba_2ZnCuF_6. *Chem. Phys.* **1991,** *155*, 117-125.
36. Steffen, G.; Reinen, D.; Stratemeier, H.; Riley, M. J.; Hitchman, M. A.; Matthies, H. E.; Recker, K.; Wallrafen, F.; Niklas, J. R., EPR and ENDOR Spectra of Copper(II) Centers with d_{z2} and d_{x2-y2} Ground-States in Ba_2ZnF_6 - Analysis of Hyperfine Parameters and Dynamic Vibronic Coupling. *Inorg. Chem.* **1990,** *29*, 2123-2131.
37. von Schnering, H. G., Kristallstrukturen der Bariumfluorometallate(II) Ba_2MF_6 mit M = Zn, Cu, Ni, Co, Fe. *Z. Anorg. Allg. Chem.* **1967,** *353*, 13-25.
38. Herdtweck, E.; Babel, D., Refinement of Crystal-Structure of K_2ZnF_4 And $K_3Zn_2F_7$. *Z. Kristallogr.* **1980,** *153*, 189-199.
39. Garcia-Lastra, J. M.; Aramburu, J. A.; Barriuso, M. T.; Moreno, M., Optical Properties of Cr^{3+}-Doped Oxides: Different Behavior of Two Centers in Alexandrite. *Phys. Rev. B* **2006,** *74*, 115118.
40. Trueba, A.; Garcia-Lastra, J. M.; Barriuso, M. T.; Aramburu, J. A.; Moreno, M., Influence of Internal Electric Fields on Bonding and Properties of Impurities in Insulators: Mn^{2+} in $LiBaF_3$ and Normal Perovskites. *Phys. Rev. B* **2008,** *78*, 075108.

41. Dovesi, R.; Orlando, R.; Erba, A.; Zicovich-Wilson, C. M.; Civalleri, B.; Casassa, S.; Maschio, L.; Ferrabone, M.; De La Pierre, M.; D'Arco, P., et al., CRYSTAL14: A Program for the Ab Initio Investigation of Crystalline Solids. *Int. J. Quantum Chem.* **2014,** *114*, 1287-1317.
42. CRYSTAL basis sets http://www.crystal.unito.it/basis-sets.php (accessed 02/09/2017).
43. Bilc, D. I.; Orlando, R.; Shaltaf, R.; Rignanese, G. M.; Iniguez, J.; Ghosez, P., Hybrid Exchange-Correlation Functional for Accurate Prediction of the Electronic and Structural Properties of Ferroelectric Oxides. *Phys. Rev. B* **2008,** *77*, 165107.
44. Velde, G. T.; Bickelhaupt, F. M.; Baerends, E. J.; Guerra, C. F.; Van Gisbergen, S. J. A.; Snijders, J. G.; Ziegler, T., Chemistry with ADF. *J. Comput. Chem.* **2001,** *22*, 931-967.
45. Stephens, P. J.; Devlin, F. J.; Chabalowski, C. F.; Frisch, M. J., Ab-Initio Calculation of Vibrational Absorption and Circular-Dichroism Spectra Using Density-Functional Force-Fields. *J. Phys. Chem.* **1994,** *98*, 11623-11627.
46. Aramburu, J. A.; Garcia-Fernandez, P.; Garcia-Lastra, J. M.; Barriuso, M. T.; Moreno, M., Colour Due to Cr^{3+} Ions in Oxides: a Study of the Model System MgO:Cr^{3+}. *J. Phys.: Condens. Matter* **2013,** *25*, 175501
47. Riley, M. J.; Hitchman, M. A.; Reinen, D., Effects of Vibronic Coupling on the Electron-Paramagnetic-Res Spectra of Copper(II) Doped K2ZnF_4. *Chem. Phys.* **1986,** *102*, 11-28.
48. Garcia-Lastra, J. M.; Barriuso, M. T.; Aramburu, J. A.; Moreno, M., Forces due to Changes of Electronic Density: a Complementary View of the Jahn-Teller Effect. *Chem. Phys.* **2005,** *317*, 103-110.
49. Aramburu, J. A.; Garcia-Fernandez, P.; Garcia-Lastra, J. M.; Moreno, M., A Genuine Jahn-Teller System with Compressed Geometry and Quantum Effects Originating from Zero-Point Motion. *Chemphyschem* **2016,** *17*, 2146-2156.
50. Moreno, M.; Barriuso, M. T.; Aramburu, J. A., Impurity-Ligand Distances Derived from Magnetic Resonance and Optical Parameters. *Appl. Magn. Reson.* **1992,** *3*, 283-304.
51. Takeuchi, H.; Arakawa, M.; Aoki, H.; Yosida, T.; Horai, K., Electron-Paramagnetic-Res and F-19-ENDOR of Cr^{3+} Impurity Centers in K_2ZnF_4 and K_2MgF_4. *J. Phys. Soc. Jpn.* **1982,** *51*, 3166-3172.
52. Garcia-Lastra, J. M.; Barriuso, M. T.; Aramburu, J. A.; Moreno, M., Cr^{3+} in Layered Perovskites: Do the Electron Paramagnetic Resonance Parameters only Depend on the Impurity-Ligand Distances? *J. Phys.: Condens. Matter* **2010,** *22*, 155502.
53. Henke, B.; Secu, M.; Rogulis, U.; Schweizer, S.; Spaeth, J. M., Optical and Magneto-Optical Studies of Mn-Activated $LiBaF_3$. *Phys. Status Solidi C* **2005,** *2*, 380-383.
54. Henry, M. O.; Larkin, J. P.; Imbusch, G. F., Nature of Broad-Band Luminescence Center in MgO-Cr^{3+}. *Phys. Rev. B* **1976,** *13*, 1893-1902.
55. Burns, R. G., *Mineralogical Applications of Crystal Field Theory*. Cambridge University Press: Cambridge, 1993.
56. Powell, R. C., *Physics of Solid State Laser Materials*. Springer: New York, 1998.
57. Sugano, S.; Tanabe, Y.; Kamimura, H., *Multiplets of Transition-Metal Ions in Crystals.* Academic Press: New York, 1970.
58. Wissing, K.; Barriuso, M. T.; Aramburu, J. A.; Moreno, M., Optical Excitations and Coupling Constants in FeO_4^{2-} and CrO_4^{4-} Complexes in Oxides: Density Functional Study. *J. Chem. Phys.* **1999,** *111*, 10217-10228.

59. Barreda-Argueso, J. A.; Aguado, F.; Gonzalez, J.; Valiente, R.; Nataf, L.; Sanz-Ortiz, M. N.; Rodriguez, F., Crystal-Field Theory Validity Through Local (and Bulk) Compressibilities in CoF_2 and $KCoF_3$. *J. Phys. Chem. C* **2016,** *120*, 18788-18793.

60. Kohn, W., Theory of Insulating State. *Physical Review* **1964,** *133*, A171-A181.

61. Resta, R.; Sorella, S., Electron Localization in the Insulating State. *Phys. Rev. Lett.* **1999,** *82*, 370-373.

62. Garcia-Fernandez, P.; Moreno, M.; Aramburu, J. A., Electrostatic Control of Orbital Ordering in Noncubic Crystals. *J. Phys. Chem. C* **2014,** *118*, 7554-7561.

63. Garcia-Fernandez, P.; Garcia-Lastra, J. M.; Trueba, A.; Barriuso, M. T.; Aramburu, J. A.; Moreno, M., Insulators Containing $CuCl_4X_2^{2-}$ (X = H_2O, NH_3) Units: Origin of the Orthorhombic Distortion Observed only for $CuCl_4(H_2O)_2^{2-}$. *Phys. Rev. B* **2012,** *85*.

64. Gazo, J.; Bersuker, I. B.; Garaj, J.; Kabesova, M.; Kohout, J.; Langfelderova, H.; Melnik, M.; Serator, M.; Valach, F., Plasticity of Coordination Sphere of Copper(II) Complexes, its Manifestation and Causes. *Coord. Chem. Rev.* **1976,** *19*, 253-297.

65. Gazo, J., Structure and Properties of Some Copper (II) Coordination-Compounds Distortion Isomerism of Copper (II) Compounds. *Pure Appl. Chem.* **1974,** *38*, 279-301.

66. Rodriguez, F., Unveiling the Local Structure of Cu^{2+} Ions from d-Orbital Splitting. Application to K_2ZnF_4: Cu^{2+} and $KZnF_3$:Cu^{2+}. *Inorg. Chem.* **2017**. **DOI:** 10.1021/acs.inorgchem.6b02677

67. Garcia-Lastra, J. M.; Barriuso, M. T.; Aramburu, J. A.; Moreno, M., Color Shift in Al_2O_3 Center·Cr(2)O(3) Solid Solutions and the Electroneutrality Principle. *Phys. Rev. B* **2009,** *79*, 241106.

68. Berke, H., The Invention of Blue and Purple Pigments in Ancient Times. *Chem. Soc. Rev.* **2007,** *36*, 15-30.

69. Garcia-Fernandez, P.; Moreno, M.; Aramburu, J. A., Origin of the Exotic Blue Color of Copper-Containing Historical Pigments. *Inorg. Chem.* **2015,** *54*, 192-199.

70. Schnering, H. G.; Kolloch, B.; Kolodzie.A, Structure of Ternary Copper(II) and Chromium(II) Fluorides. *Angew. Chem., Int. Ed.* **1971,** *10*, 413-+.

Host Lattice	R_{ax}^0 (pm)	R_{eq}^0 (pm)	R_{av}^0 (pm)	Δ (eV)
K_2ZnF_4	202.6	202.9	202.8	0.70
Ba_2ZnF_6	196.7	205.0	202.2	0.80

Table 1. Experimental values of Zn^{2+}-F^- distances in the perfect host lattice for K_2ZnF_4 [38] and Ba_2ZnF_6 [35-36] layered perovskites. The axial Zn^{2+}-F^- distance, R_{ax}^0, is that along the crystal **c** axis (Figure 1) while R_{eq}^0 corresponds to the layer plane and R_{av}^0 is the average value. The gap energy, Δ, between the $b_{1g}(\sim x^2-y^2)$ and $a_{1g}(\sim 3z^2-r^2)$ levels measured for both $K_2ZnF_4:Cu^{2+}$ [19, 21] and $Ba_2ZnF_6:Cu^{2+}$ [35] is also reported.

	Experimental	Calculated		
		Periodic	49 ion cluster	109 ion cluster
R_{eq}^0	205.0	204.7	203.8	204.3
R_{ax}^0	196.7	195.9	197.1	200.7
a	410.1	409.3	-	-
c	1626.3	1617.3	-	-

Table 2. Comparison of *a* and *c* lattice parameters, and the axial, R_{ax}^0, and equatorial, R_{eq}^0, Zn^{2+}-F^- distances corresponding to pure Ba_2ZnF_6 derived through periodic and cluster calculations with those obtained from X-ray diffraction data[37]. All distances are given in pm units.

System	Calculation	State	R_{eq}	R_{ax}	R_{eq} - R_{ax}	R_m	ΔE
$K_2ZnF_4:Cu^{2+}$	Periodic	A_{1g}	204.3	193.1	11.2	200.6	-
$Ba_2ZnF_6:Cu^{2+}$	Periodic	A_{1g}	207.0	188.5	18.5	200.8	-
	Cluster	A_{1g}	207.5	191.9	15.6	202.3	-0.65
	Cluster	B_{1g}	201.4	207.8	-6.4	203.5	-0.09
	Cluster	$b_{1g}^{1.5}a_{1g}^{1.5}$	205.0	199.6	5.4	203.2	0

Table 3. Calculated values of equilibrium axial, R_{ax}, and equatorial, R_{eq}, Cu^{2+}-F^- distances, for CuF_6^{4-} complexes formed in Ba_2ZnF_6 and K_2ZnF_4 host lattices using periodic and 49 ion cluster calculations. Periodic calculations always converge to the ground state A_{1g}. Cluster calculations in $Ba_2ZnF_6:Cu^{2+}$ have been performed for the ground state A_{1g}, the excitated estate B_{1g} and also the reference state with electronic configuration $b_{1g}^{1.5}a_{1g}^{1.5}$. Values of the tetragonal distortion, R_{eq} - R_{ax}, and the mean distance, $R_m = (R_{ax} + 2R_{eq})/3$, are also given for comparison. All distances are in pm. ΔE is the calculated energy difference (in eV) with respect to the reference $b_{1g}^{1.5}a_{1g}^{1.5}$ state.

Transition	Isolated CuF_6^{4-}	CuF_6^{4-} under $\mathbf{E}_R(r)$	Experimental
$b_{1g}(\sim x^2-y^2) \rightarrow a_{1g}(\sim 3z^2-r^2)$	0.53	0.93	0.80
$e_g(\sim xz,yz) \rightarrow a_{1g}(\sim 3z^2-r^2)$	1.15	1.24	1.18
$b_{2g}(\sim xy) \rightarrow a_{1g}(\sim 3z^2-r^2)$	1.31	1.61	1.61

Table 4. Energy values (in eV) of the three *d-d* transitions calculated for the tetragonal CuF_6^{4-} unit formed in Ba_2ZnF_6 at the equilibrium geometry. In addition to results derived for the isolated complex those obtained including the effects of the internal electric field, $\mathbf{E}_R(r)$, are displayed as well. The experimental optical transitions measured for CuF_6^{4-} in Ba_2ZnF_6 [35] are also enclosed for comparison.

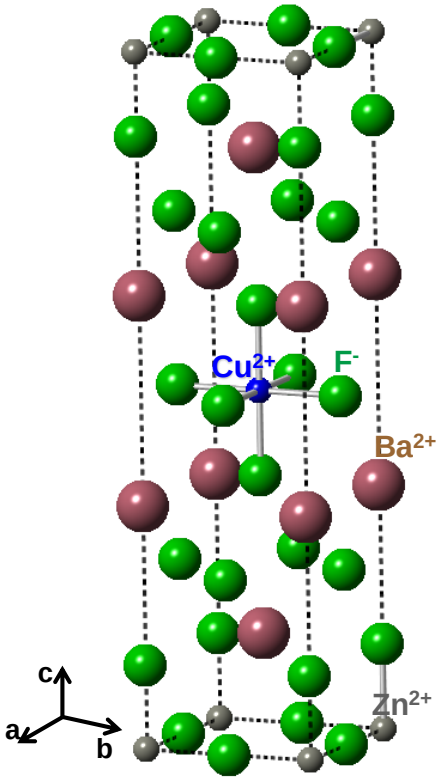

Figure 1. Unit cell of Ba_2ZnF_6 layered perovskite showing the Cu^{2+} centre I corresponding to a CuF_6^{4-} complex.

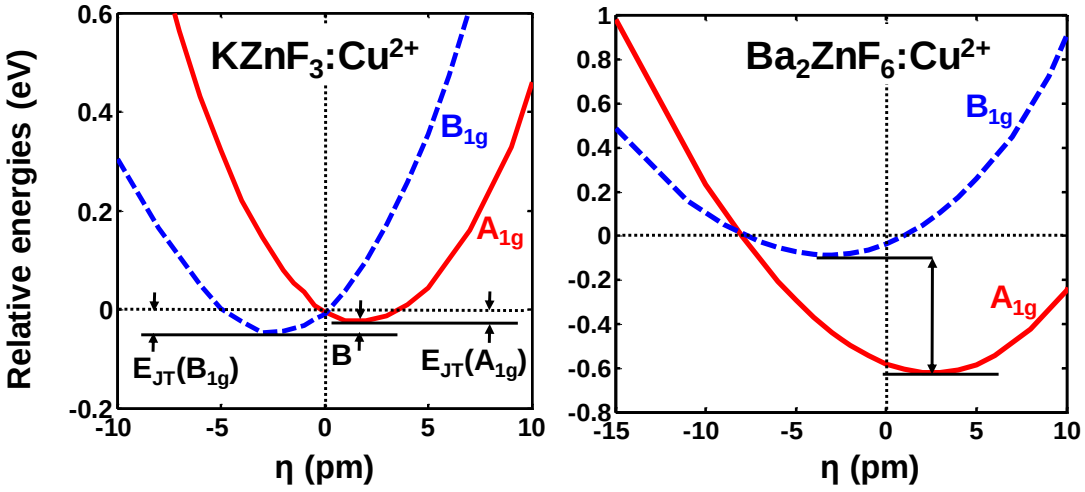

Figure 2. Adiabatic Potential Energy Surface (APES) obtained in DFT calculations on a 57 ion cluster simulating $KZnF_3:Cu^{2+}$ and on a 49 ion cluster simulating $Ba_2ZnF_6:Cu^{2+}$ by constraining the occupation of the orbitals to obtain A_{1g} ($b_{1g}^2a_{1g}^1$ configuration) and B_{1g} ($a_{1g}^2b_{1g}^1$) states. Calculations have been carried as a function of a JT distortion coordinate η, defined by $R_{eq} = R_{eq}(av) \pm \eta$ y $R_{ax} = R_{ax}(av)$ μ 2η, where $R_{eq}(av)$ and $R_{ax}(av)$ are the optimized Cu^{2+}-F^- distances for the average reference state with configuration $b_{1g}^{1.5}a_{1g}^{1.5}$. Note the different scales used for the two systems. Dotted lines correspond to the geometry and energy of the average reference states.

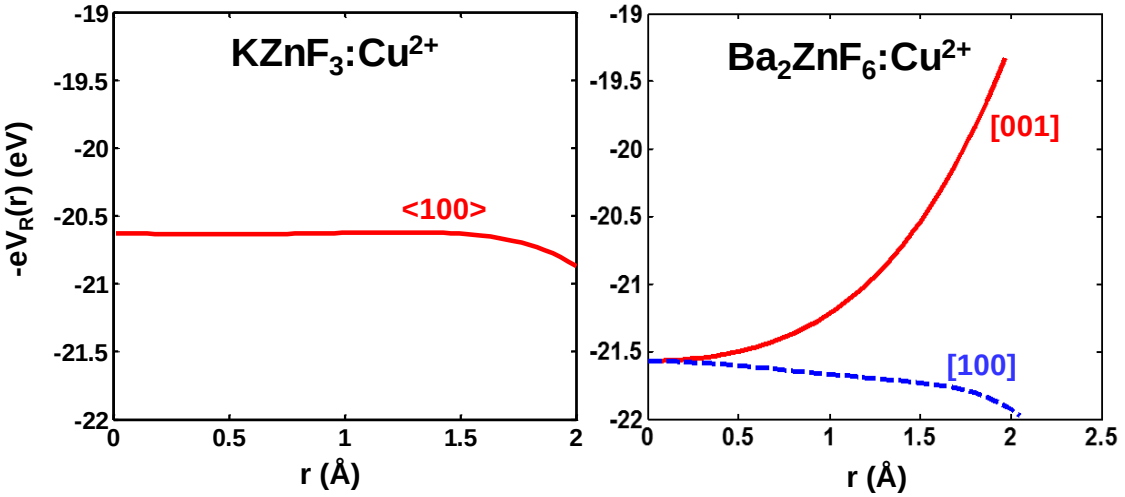

Figure 3. Behavior of the energy (-*e*)V_R(**r**) associated with the electrostatic potential, V_R(**r**), produced on a 7 atom CuF_6^{4-} complex by the rest of ions on the cubic $KZnF_3$ lattice and the tetragonal Ba_2ZnF_6 lattice. In this later case the quantity (-*e*)V_R(**r**) is depicted along [100] and [001] crystalline directions.

TOC Graphic

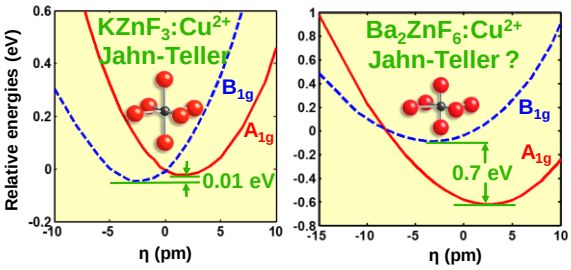
KZnF3:Cu2+
Jahn-Teller
B1g
A1g
0.01 eV
Relative energies (eV)
η (pm)
Ba2ZnF6:Cu2+
Jahn-Teller ?
B1g
A1g
0.7 eV
η (pm)